8B.4 RANGE CORRECTION FOR RADAR-DERIVED AZIMUTHAL SHEAR: APPLICATIONS TO A TORNADO DETECTION ALGORITHM

Jennifer F. Newman[1*], Valliappa Lakshmanan[2], Pamela L. Heinselman[3], and Travis M. Smith[2]
[1]School of Meteorology, University of Oklahoma, Norman, OK
[2]Cooperative Institute for Mesoscale Meteorological Studies, University of Oklahoma, Norman, OK
[3]NOAA/National Severe Storms Laboratory, Norman, OK

1. INTRODUCTION

Since the 1940s, weather radar has proven to be an invaluable tool in the prediction and detection of tornadoes. Austin (1945) was the first to use incoherent radar to document the classical "hook echo" signature, which forms in conjunction with the rear flank downdraft of a supercell. Hook echoes were later associated with tornadoes (e.g., Stout and Huff 1953; Fujita 1958). However, a study by Forbes (1981) determined that not all tornadoes are associated with a hook echo signature, or any sort of reflectivity signature, highlighting the need for radial velocity measurements and pulsed Doppler radar.

Observations of tornadoes using Doppler radar during the 1960s and 1970s led to the discovery of the Tornadic Vortex Signature (TVS) in radial velocity data. The TVS, defined as a significant velocity difference at adjacent radials at the same range, often develops at midaltitudes prior to the development of a tornado and descends toward the ground in classic supercell tornado cases (Burgess et al. 1975; Brown et al. 1978).

The discovery of the TVS and the establishment of the Weather Surveillance Radar-1988 Doppler (WSR-88D) network greatly improved tornado warning performance during the early 1990s (Polger et al. 1994), and preliminary circulation detection algorithms for the WSR-88D system were developed. Further research and improved computing capabilities led to the development of more sophisticated algorithms during the latter half of the decade (e.g., Mitchell et al. 1998). However, the circulation detection algorithms currently in use with the WSR-88D system are still prone to high false alarm ratios (Jones et al. 2004). Many false detections are caused by ground clutter targets and aliasing in the velocity field (Jones et al. 2004). The need for a radar-derived shear quantity that is more immune to dealiasing errors and noisy data prompted the development of the local, linear least squares derivatives (LLSD) method for estimating azimuthal shear (Smith and Elmore 2004).

The LLSD method estimates shear using derivatives of the velocity field in neighborhoods of different sizes. In contrast, the commonly used peak-to-peak method simply uses the difference between two peak velocity values in regions of high velocity gradients to estimate shear. Peak-to-peak shear estimates are strongly affected by range from the radar, noise, and beam position in relation to the circulation center; however, LLSD shear is less dependent on radar location and could potentially serve as a valuable parameter for tornado detection (Smith and Elmore 2004).

In this work, the use of LLSD shear to detect circulations in Doppler radar data is explored. Since LLSD shear appears to show some range dependence, a regression equation is developed to correct LLSD shear for range degradation. The range correction is applied to radar data from two tornado cases and corrected shear is compared to the original shear field.

2. BACKGROUND

We are currently developing a circulation detection algorithm which uses LLSD shear. This algorithm is somewhat similar to other techniques used in tornado detection algorithms but employs different methods to associate shear regions in space and time.

2.1. *Tornado Detection Algorithms*

Initially, development of an operational tornado detection algorithm (TDA) was limited by

* *Corresponding author address:* Jennifer F. Newman, School of Meteorology, University of Oklahoma, 120 David L. Boren Blvd., Norman, OK 73072. E-mail: jennifer.newman@ou.edu

Doppler radar data availability and computing resources. Prior to the deployment of the WSR-88D network, most Doppler radar data from tornado cases was collected in Oklahoma from mesocyclonic storms (Stumpf et al. 1998). Thus, early TDAs (e.g., Zrnić et al. 1985; Donaldson and Desrochers 1990) were developed, trained, and tested using only a few tornado cases from a specific geographic area. However, these initial TDAs performed well on the Oklahoma tornado cases and some of the techniques developed are still commonly used in TDAs.

The TDA currently used with the WSR-88D system (Mitchell et al. 1998) emphasizes the difference between velocity values at constant range and adjacent azimuths; if this velocity difference exceeds a particular threshold, the gate pair is saved as a shear segment. Shear segments are then associated in range and height. An aspect ratio check is included to eliminate elongated shear regions associated with gust fronts or other nontornadic regions. Three-dimensional features are either classified as TVSs or elevated TVSs. Detected circulations are tracked and trend and strength information is displayed.

Liu et al. (2007) discuss several issues related to using the gate-to-gate velocity difference to detect tornadoes. The actual value of this difference can be affected by the azimuthal offset of the radar beam center from the vortex (e.g., Wood and Brown 1997), as well as noisy data and velocity aliasing. In addition, the azimuthal resolution degrades with range as the radar beam widens, leading to less accurate velocity measurements at far ranges. To mitigate these issues, Liu et al. (2007) propose using a wavelet analysis technique to measure the average velocity difference between regions of different scales. This technique utilizes velocity data at several different points, so it is less susceptible to noisy or inaccurate data. It also considers circulations at a variety of scales, and thus can detect both tornado- and mesocyclone-scale circulations.

Yu et al. (2007) suggest the use of Doppler spectra to identify tornadic regions in the radial velocity field. Unlike the TVS, Yu et al. (2007) argue that characteristics of a tornadic Doppler spectrum do not degrade significantly with range, making them ideal for tornado detection. Following the results of Yu et al. (2007), Wang et al. (2008) developed a TDA that uses spectral signatures and a fuzzy logic system to make detections. By examining histograms of different variables from two Oklahoma cases, Wang et al. (2008) determined that values of these variables overlapped significantly for tornadic and nontornadic scans. Thus, instead of simply adopting thresholds, Wang et al. (2008) suggest using a fuzzy logic system to integrate variables.

Since time-series data are not currently available operationally, the Wang et al. (2008) TDA can only be applied to a few tornado cases. However, Wang and Yu (2009) modified this TDA for a typical operational WSR-88D radar. Different versions of the Wang et al. (2008) TDA were developed that accepted different combinations of variables, depending on whether time-series, polarimetric, or solely moment data were available.

2.2. *LLSD Shear*

Estimates of azimuthal shear that use the difference between peak velocity values can be affected by radar beam location and noisy data, as discussed in the previous section. This "peak-to-peak" azimuthal shear estimate is given by the following equation:

$$shear_{ptp} = \frac{V_{max} - V_{min}}{d} \tag{1}$$

V_{max} and V_{min} are the maximum and minimum velocities associated with the circulation, respectively, and d is the distance between them. As an alternative to the peak-to-peak shear calculation, Elmore et al. (1994) propose a method of estimating the derivatives of radial velocity values. This method involves fitting a plane to the velocity field and finding the slope of that plane, or equivalently, estimating the azimuthal derivative of the velocity.

An estimate of the azimuthal derivative of the radial velocity is given by

$$\frac{\partial V_r}{\partial \theta} = \frac{\sum s_{ij} V_{ij} w_{ij}}{\sum (\Delta s_{ij})^2 w_{ij}} \tag{2}$$

where V_r is the radial velocity, θ is the azimuth angle, s_{ij} is the distance from the point where the calculation is being evaluated to the point (i, j) in the neighborhood of the point of interest, V_{ij} is the radial velocity at (i, j), and w_{ij} is a weight function. This estimate of the azimuthal shear is known as the *local, linear least squares derivatives (LLSD) method*.

Smith and Elmore (2004) applied the LLSD shear estimate to simulated and observed circulations. First, the velocity data were passed through a 3x3 median filter to eliminate noise. Next, Equation 2 was applied to the filtered velocity data to estimate the azimuthal shear. The radial and azimuthal dimensions of the kernel used in the calculation were held constant, such that fewer radials were used in the calculation at far ranges.

Smith and Elmore (2004) simulated circulations of varying strengths and diameters at ranges from 20 to 200 km, adopting the Rankine vortex simulation described by Wood and Brown (1997). Noise was added to the velocity data and random azimuthal offsets from the beam centerline were added to the circulation location to simulate real sampling limitations. For each range, 1000 circulations were simulated with different noise values and azimuthal offsets, and mean and 95% confidence intervals were calculated for LLSD and peak-to-peak shear. Calculations for a 5-km diameter vortex using a 2.5-km azimuthal kernel indicated that the LLSD shear value is within 20% of its true value out to a range of ~140 km, with a much smaller variance than peak-to-peak shear.

In addition, azimuthal position errors were examined for the two shear calculations. For peak-to-peak shear, the circulation center was assumed to be located halfway between the peak maximum and minimum velocity values, while for LLSD shear, the circulation center was assumed to be collocated with the shear maximum. The azimuthal position errors for LLSD shear were much smaller, particularly at far ranges.

Since LLSD shear utilizes velocity data at multiple points, it is less susceptible to noise and velocity aliasing. LLSD shear estimates also display less variance at far ranges in comparison to peak-to-peak shear, as shown by Smith and Elmore (2004). Since LLSD shear degrades with range, a range-dependent threshold would be necessary for a TDA that uses LLSD shear. In this paper, a range correction is applied to LLSD shear values such that a single threshold can ideally be used to detect significant circulations at all ranges.

2.3. *Identifying and Tracking Shear Clusters*

The circulation detection algorithm currently being developed at NSSL uses the LLSD shear field as an input parameter. This algorithm (hereafter LLSD TDA) first segments the LLSD shear field into clusters of local shear maxima, then produces motion estimates and attempts to track these clusters with time.

Clusters are initially identified using the extended watershed transform developed by Lakshmanan et al. (2009). Starting at a local maximum, an azimuthal shear region is grown until it reaches a specific size threshold. Size thresholds and upper and lower limits for the local maxima are user-specified; local maxima below the lower threshold are not used to form shear clusters.

The motion estimate for each cluster is found by minimizing the mean absolute error between the cluster in the current scan and corresponding pixels in the previous scan; whichever motion vector minimizes this error is selected as the best motion estimate (Lakshmanan et al. 2003). After motion estimates have been produced, clusters are associated in time (Lakshmanan and Smith 2010).

The LLSD TDA is the first circulation detection algorithm to incorporate the LLSD shear field. LLSD shear and divergence have previously been used in a downburst detection algorithm (Smith et al. 2004). LLSD shear has also been used to estimate vorticity from phased array radar data for a reintensifying supercell case (Heinselman et al. 2008).

Similar to the wavelet TDA (Liu et al. 2007), the LLSD TDA identifies circulations at different scales using size thresholds. The LLSD TDA also utilizes velocity data at several different points to make shear calculations, as in Liu et al. (2007). Since pixels are added to shear clusters in the LLSD TDA until the clusters reach a size threshold, there is no need to associate shear segments in range and azimuth to create shear regions (e.g., Zrnić et al. 1985; Stumpf et al. 1998). Adjacent shear clusters within a user-specified distance may be combined in the LLSD TDA to reach the size threshold.

Like the NSSL MDA, the LLSD TDA projects shear clusters in time using the estimated motion vector and uses a search radius to associate clusters in time. The NSSL MDA uses either the previous motion vector of the circulation centroid or the average of all the circulation motion vectors in the previous volume scan. In contrast, the LLSD TDA minimizes the error between projected and actual cluster locations in the current scan to produce motion estimates. Further LLSD TDA developments could incorporate machine learning techniques, such as neural networks and fuzzy logic, to make circulation detections.

2.4. *Resolution Correction Techniques*

Donaldson and Desrochers (1990) and Desrochers and Donaldson (1992) apply resolution corrections to circulation diameters and velocities to mitigate effects of limited radar resolution. The correction factors, based on the work of Brown and Lemon (1976), depend on the beamwidth to core radius ratio (BW/CR).

Chumchean et al. (2004) apply a range correction to radar reflectivity to correct the range-dependent bias in rainfall estimates. Like velocity estimates, reflectivity estimates are also affected by the increase in radar resolution volume with range; at far ranges, small features in the reflectivity field are "smoothed out" because of the increased beamwidth. However, a range correction has not yet been applied to azimuthal shear estimates.

3. TORNADO CASES

Radar data for 31 confirmed tornadoes were used to examine the effects of tornado strength and range on LLSD shear signatures. These tornadoes encompassed a variety of geographical regions and convective modes. Tables 1 and 2 summarize the locations and strengths of the tornadoes used in the study. The distribution was heavily weighted toward weaker tornadoes (EF0 and EF1), since it is likely that the shear signatures of these tornadoes are strongly affected by range. In addition, weak tornadoes tend to occur more frequently, while EF4 and EF5 tornadoes are exceedingly rare (e.g., Trapp et al. 2005). Thus, the tornadoes selected for the study roughly represent the climatological distribution of tornadic intensity.

3.1. *Extracting Shear Values*

Tornadoes were analyzed using Doppler radar data from the nearest WSR-88D radar for each case. Paths were determined by tracking regions of maximum LLSD shear, using ground truth reports for guidance where available. For each volume scan and elevation angle, an algorithm searched for the maximum LLSD shear value within a 5-km radius of a user-specified point. To allow for a possible increase in circulation size with height, the search radius was expanded to 7.5 km at upper levels.

Tornadoes were tracked from roughly 10 min before the first damage report to ten minutes after the last damage report. The maximum LLSD shear value for each volume scan was defined as the maximum shear value that was measured below 3 km while confirmed tornado damage was occurring. For tornadoes at far ranges, values from the 0.5° elevation angle were used. The "precursor" LLSD shear value was defined as the lowest maximum LLSD shear value that occurred in the 10 min prior to tornado damage reports. This precursor value could potentially serve as a shear threshold for a circulation detection algorithm.

3.2. *Distribution of Shear Values*

Fig. 1 shows the normalized frequency of maximum and precursor shear values for the data set. The number of tornadoes in each shear bin was normalized by the total number of tornadoes used for the histogram. Figs. 1c and d show the LLSD shear frequencies separated by tornado range from the radar.

Both the maximum and the precursor shear values display a Gaussian-like distribution, with the majority of tornadoes producing intermediate shear values and a few tornadoes producing low and high shear values. When separated by range, the histograms reveal a potential range bias. The shear values at closer ranges tend to be higher than the shear values at far ranges. Since the percentage of weak tornadoes in the study at each range interval is roughly the same (see Table 2), it's likely that shear degradation with range is primarily responsible for the discrepancies in the histograms. This difference is even more evident for the shear precursor values (Fig. 1d).

Histograms for EF0 and EF1 tornadoes reveal significant overlap in the shear values for the weakest tornadoes (Figs. 1e and f). This overlap could be an issue for a forecaster or radar operator trying to estimate tornado strength from LLSD shear data. An EF1 tornado could produce significantly more damage than an EF0 tornado, and hypothetically should have a correspondingly higher LLSD shear value. Ideally, LLSD shear magnitude would increase with increasing tornado strength, but this is not the case when the shear signature has been affected by range and other radar-dependent parameters.

Cumulative frequency distributions (CFDs) were also calculated for the maximum and precursor shear values. The cumulative frequency for a particular shear value can be interpreted as the probability that an arbitrary future shear value will

be lower than this shear value (Wilks 2006). The Tukey estimator (Wilks 2006) was used to calculate the CFD functions.

Fig. 2 shows the graphs of the CFD functions. The intersection of the 10% probability line with the CFD reveals the shear value which 90% of future tornadic shear values are expected to exceed. Thus, this shear value could be used as a threshold in a circulation detection algorithm. Based on the distribution in Fig. 2, the maximum and precursor "threshold" LLSD shear values are 0.01 s^{-1} and 0.008 s^{-1}, respectively. However, Figs. 2c and d reveal that this threshold shear value is strongly range-dependent. The difference between the 0–50 km and 100–150 km shear threshold values is nearly 0.01 s^{-1}. Since LLSD shear is generally only on the order of 0.01 s^{-1} for mesocyclone-scale circulations (Smith and Elmore 2004), this range dependence is a significant issue. The range dependence of the shear thresholds garnered from the CFD functions was the motivation for a shear range correction.

4. RANGE CORRECTION FOR LLSD SHEAR

Two equations (a "near-range" equation and a "far-range" equation) were developed to correct LLSD shear values for degradation due to range from the radar. Thousands of Rankine vortices were simulated and used as input for a regression equation relating measured circulation parameters to true azimuthal shear.

Various mesocyclone-scale circulations were simulated using the technique described by Wood and Brown (1997). This simulation creates modified Rankine (1901) vortices with user-specified peak velocities, core diameters, and ranges. The vortices are then sampled by a simulated WSR-88D radar. Gaussian-distributed noise is added to the velocity values and random azimuthal offsets from the beam centerline are added to the circulation center location.

For this work, simulated diameters ranged from 1 to 4 km in increments of 0.25 km, and peak velocities ranged from 20 to 50 m s^{-1} in increments of 2 m s^{-1}. A radar with a 0.5° azimuthal sampling interval and a 1.02° effective beamwidth was used. For each circulation, 1000 simulations were produced with different noise patterns at ranges from 5 to 140 km in increments of 5 km. Mean values of parameters were calculated from the 1000 iterations and used to develop the equations.

A multiple linear regression technique (Draper and Smith 1998) was used to develop the range correction equations. The predictors in the equations are LLSD shear value, measured peak velocity, the inverse of the estimated diameter, and range. The circulation diameter was estimated by finding the distance between peak positive and negative velocity values.

The output of the equation is an estimate of the "true" azimuthal shear. This true value is assumed to be the same as the peak-to-peak shear value, calculated using the true peak velocity and diameter values.

4.1. *Selecting Diameters for Regression Equations*

Before the regression equations were developed, the shear degradation of circulations of different diameters was examined. If the measured shear values from a particular circulation are not significantly different from the true shear value, there is no need to apply a shear correction.

Since LLSD shear values are generally on the order of 0.01 s^{-1} (Smith and Elmore 2004), a measured shear value that was more than 0.01 s^{-1} different from the true shear value was declared to need a range correction. Shear error, defined as the difference between the true and measured shear values, was plotted for different diameters and ranges (Fig. 3). In general, error increases with increasing peak velocity and range. These plots were used to determine at what range a correction would first be needed for each diameter. For circulations with diameters greater than or equal to 3 km, a range correction is not needed through a range of 140 km. Thus, only circulations with diameters from 1 to 2.75 km were used to develop the regression equations. Since the lowest elevation angle on a WSR-88D radar scans the atmosphere at ~2.4 km above radar level at a range of 140 km, radar data beyond this range would likely not be used to detect low-level mesocyclones.

4.2. *Resolution Issues*

Clearly, a circulation with a 1-km diameter will not be resolved at a range of 140 km. The minimum resolvable diameter at a particular range is limited by the beamwidth of the radar, which widens with range. Since the regression equations rely upon an accurate diameter measurement, a

range correction can only be applied to circulations that are well-resolved.

The mean estimated diameter was calculated for circulations with different peak velocities, ranges, and true diameter values. If the estimated diameter differed from the true diameter by more than 10% at six or more velocities for a circulation at a particular range, the circulation was declared unresolvable at that range. Unresolvable circulations were not included in the regression equation.

4.3. *Resulting Equations*

When all diameters between 1 and 2.75 km were included in a regression equation, the equation performed well for larger diameters but poorly for the smallest diameters. Thus, two separate equations were developed — a "near" equation for smaller diameters and a "far" equation for larger diameters. The near equation can only be applied at ranges out to 85 km, while the far equation can be applied out to 135 km. Diameters from 1 to 1.75 km were used to develop the near equation and diameters from 2 to 2.75 km were used to develop the far equation. The diameters for the two equations were selected by examining the resolvable ranges for each diameter. A 1.75-km diameter circulation is only resolvable at ranges less than 85 km, while a 2-km diameter circulation is resolvable out to 100 km. This large difference in resolvable ranges was used to separate the diameters into two different equations.

The final near-range equation is:

$$s^* = -0.0734 + 0.0872D^{-1} + 0.00179V - 0.0884s + 0.000248r$$

where s^* is the corrected shear, D is the diameter in km, V is the maximum measured velocity in m s^{-1}, s is the LLSD shear in s^{-1}, and r is the range in km. The near equation can be applied at ranges out to 85 km for diameters between 1 and 1.75 km with the following stipulations:

If Range $\geq$ 50 km, Diameter must be $\geq$ 1.25 km
If Range $\geq$ 65 km, Diameter must be $\geq$ 1.5 km
If Range $\geq$ 75 km, Diameter must be $\geq$ 1.75 km

These stipulations correspond to the the minimum resolvable scale at each range.

The final far-range equation is:

$$s^* = -0.0431 + 0.0855D^{-1} + 0.000921V + 0.0723s + 9.97e^{-5}r$$

The far equation can be applied at ranges out to 135 km for diameters between 2 and 2.75 km with the following stipulations:

If Range $\geq$ 100 km, Diameter must be $\geq$ 2.25 km
If Range $\geq$ 110 km, Diameter must be $\geq$ 2.5 km
If Range $\geq$ 120 km, Diameter must be $\geq$ 2.75 km

The results for the near and far equations are shown in Fig. 4. There are several corrected shear estimates for every true shear value, because corrected shear values for all ranges are shown — the different shear estimates correspond to different ranges.

The R^2 (Wilks 2006) values for both the near and far equations are fairly high — 0.9648 and 0.980, respectively. The near equation performed the most poorly for the strongest and weakest 1-km diameter circulations. The far equation performed the most poorly for the strongest 2-km diameter circulations (velocity $>$ 45 m s^{-1}) at far ranges. For both equations, the regression appeared to show the most skill for circulations of intermediate diameters and velocities.

4.4. *Application of the Regression Equations*

Before the regression equations are applied to circulations in real radar data, a set of rules regarding the range and estimated size of the circulation must be established such that the appropriate equation is used. This set of rules is illustrated in the flowchart on the next page. The range correction is only applied to circulations that are resolvable and need a correction.

Several practical issues limit the effectiveness of the range correction equations. First, the equations assume that the circulation can be modeled as a Rankine vortex, which is often not true in nature (e.g., Desrochers and Harris 1996). Second, diameter estimates are limited by the width of the radar beam; thus, the diameters of small circulations can be easily overestimated, particularly at ranges far from the radar. For example, a 1-km vortex could appear as a 1.75-km vortex if it is located at a far range, and the output of the range correction equation would be inaccurate. However, any range-corrected value would tend to be closer to the circulation's true shear value, even if the diameter estimate is inaccurate.

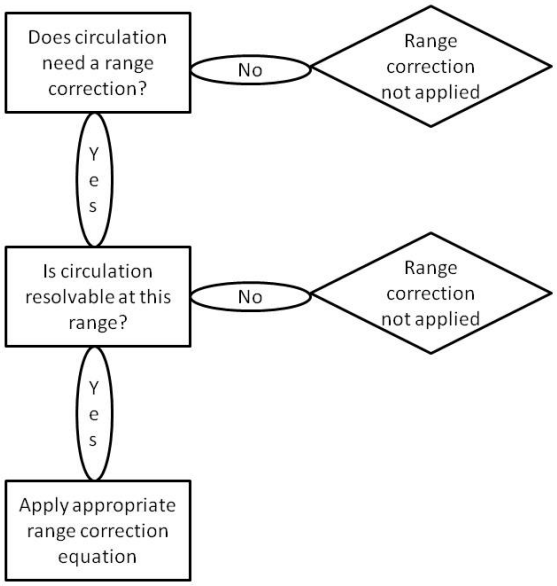

5. APPLYING RANGE CORRECTION TO REAL DATA

The range correction equations were applied to LLSD shear data from two tornado cases in the initial test set — the 10 February 2009 event in Oklahoma and the 22 October 2009 event in Louisiana. Both events were sampled by a WSR-88D radar operating in super-resolution mode (KTLX in Twin Lakes, Oklahoma and KLCH in Lake Charles, Louisiana). LLSD shear was calculated using the velocity data from both events. Maximum LLSD shear, peak velocity, and estimated diameter values from the 0.5° elevation angle were extracted along tornado tracks and used as input for the range correction equations.

5.1. *10 February 2009 — Oklahoma*

On 10 February 2009, a strong upper-level trough moved through the Southern Plains region. Low-level moisture was advected from the Gulf of Mexico and a surface dryline was established during the day. A midlevel jet aided in the development of strong low-level shear and enhanced the likelihood for supercell and tornado formation. Several supercells formed in central and western Oklahoma and spawned tornadoes. A cyclic supercell moved through the western side of Oklahoma City and produced at least three tornadoes during its lifetime.

The cyclic supercell was tracked for one hour, as it produced an EF1 tornado, an EF2 tornado, and an EF0 tornado, and maximum shear values were extracted. Since the estimated circulation diameter was less than 1 km for several volume scans, it's likely that the shear values at these times are more representative of a tornado, rather than the surrounding mesocyclone.

Fig. 5 shows the results from the range correction. Most of the corrected shear values are nearly an order of magnitude larger than the original LLSD shear values. Furthermore, the tornado formation times are more readily apparent from the temporal trends in the corrected shear. The supercell produced tornadoes at approximately 20:34, 20:53, and 21:23 UTC. These times correspond well to peaks in the corrected shear plot; this signal is not as clear in the noisier original LLSD shear field. In addition, the relative magnitudes of the peak corrected shear values roughly correspond to tornado intensity. The tornado intensity and formation times include an EF1 tornado at 20:34 UTC, an EF2 tornado at 20:53 UTC, and an EF0 tornado at 21:23 UTC. The peak corrected shear values during the time of the EF2 tornado are much larger than the peak corrected shear values during the time of the EF0 tornado.

5.2. *22 October 2009 — Louisiana*

On 22 October 2009, the remnants of an Atlantic hurricane moved through Louisiana, supplying moisture and upper-level divergence. During the morning and early afternoon of 22 October, central/southern Louisiana was located in the warm sector of a surface low pressure system. A low-level jet enhanced low-level shear, and rotating storms were forecasted by the Storm Prediction Center.

Although the primary convective mode was quasi-linear, a few supercells formed in southeastern Louisiana and produced tornadoes. One of these supercells was tracked for two hours as it produced five tornadoes — three EF0 tornadoes and two EF1 tornadoes. The supercell was located at ranges between 45 and 92 km from KLCH when it was tracked.

The range correction results are shown in Fig. 6. Tornadoes were produced at approximately 17:05, 17:22, 17:47, 18:05, and 18:15 UTC. The second and third tornadoes were rated EF1, and the remaining tornadoes were rated EF0.

The measured shear values between 17:30 and 18:15 UTC are significantly smaller than those

measured during the beginning of the data set. At the end of the supercell's lifetime, it had started moving away from KLCH; this difference in range could explain the difference in measured shear magnitude. The range difference did not appear to have a significant impact on the corrected shear values.

Similar to the Oklahoma case, the corrected shear values are nearly an order of magnitude larger than the original shear values. Again, the peaks in the corrected shear values correspond fairly well to tornado formation times. The original shear values show this trend to some extent as well, although the peaks in the original shear are not as well-defined. This discrepancy can be partially attributed to the range of shear values present in the original and corrected shear fields. The larger jumps in the corrected shear field make it easier to differentiate between tornadic and nontornadic time periods.

Unlike the Oklahoma case, tornado strength could not be easily discerned from either the original or corrected shear magnitudes. In fact, the first tornado, rated EF0, produced the highest corrected shear values of the entire time period. National Weather Service storm reports for the event indicate that a few of the tornadoes either occurred in rural areas or occurred in areas that were difficult to access due to heavily forested regions. These factors suggest that the intensities of the tornadoes for this event were likely difficult to assess, and as a result, the reported tornado intensities may not be entirely accurate.

6. SUMMARY

The LLSD shear method was introduced and related to previously used tornado detection techniques. Since LLSD shear is less radar-dependent than peak-to-peak shear, it could potentially be used to detect circulations with significant skill. In addition, the LLSD shear method is not strongly affected by noisy velocity data, since it utilizes a region in the velocity field, rather than just a few points.

The LLSD shear signatures for 31 tornadoes were examined and stratified by range from the radar. It was revealed that if a simple thresholding scheme was used to make circulation detections, this LLSD shear threshold would depend upon range from the radar. Regression equations were developed to correct LLSD shear for range degradation, and the resulting range correction was applied to LLSD shear values from two tornadic storms. The range correction increased shear values by nearly an order of magnitude and made it easier to differentiate between tornadic and nontornadic radar scans.

In the future, the range-corrected shear will be used to detect circulations in Doppler radar data and comparisons will be made to more commonly used peak-to-peak shear techniques.

7. ACKNOWLEDGMENTS

Funding for the authors was provided under NOAA-OU Cooperative Agreement NA17RJ1227. The authors would like to thank Bim Wood and Rodger Brown for their assistance with the Rankine vortex simulation.

8. REFERENCES

Austin, G., 1945: Forecasting the maintenance of mesoscale convective systems crossing the Appalachian Mountains. *Weather Service Bulletin*, **3**, 1179–1195.

Brown, R. A. and L. R. Lemon, 1976: Single Doppler radar vortex recognition: Part 2: Tornadic vortex signatures. Preprints, *17th Conf. on Radar Meteorology*, Seattle, WA. Amer. Meteor. Soc., 104–109.

Brown, R. A., L. R. Lemon, and D. W. Burgess, 1978: Tornado detection by pulsed Doppler radar. *Mon. Wea. Rev.*, **106**, 29–38.

Burgess, D. W., L. R. Lemon, and R. A. Brown, 1975: Tornado characteristics revealed by Doppler radar. *Geophys. Res. Lett.*, **2**, 183–184.

Chumchean, S., A. Seed, and A. Sharma, 2004: Application of scaling in radar reflectivity for correcting range-dependent bias in climatological radar rainfall estimates. *J. Atmos. Oceanic Technol.*, **21**, 1545–1556.

Desrochers, P. R. and R. J. Donaldson, 1992: Automatic tornado prediction with an improved mesocyclone-detection algorithm. *Wea. Forecasting*, **7**, 373–388.

Desrochers, P. R. and F. I. Harris, 1996: Interpretation of mesocyclone vorticity and divergence structure from single-Doppler radar. *J. Appl. Meteor.*, **35**, 2191–2209.

Donaldson, R. J. and P. R. Desrochers, 1990: Improvement of tornado warnings by Doppler radar measurement of mesocyclone rotational kinetic energy. *Wea. Forecasting*, **5**, 247–258.

Draper, N. R. and H. Smith, 1998: *Applied Regression Analysis*. Wiley, 706 pp.

Elmore, K. M., E. D. Albo, R. K. Goodrich, and D. J. Peters, 1994: *NASA/NCAR airborne and ground-based wind shear studies. Final report, contract no. NCC1-155*. 343 pp.

Forbes, G. S., 1981: On the reliability of hook echoes as tornado indicators. *Mon. Wea. Rev.*, **109**, 1457–1466.

Fujita, T., 1958: Mesoanalysis of the Illinois tornadoes of 9 April 1953. *Journal of Meteorology*, **15**, 288–296.

Heinselman, P. L., D. L. Priegnitz, K. L. Manross, T. M. Smith, and R. W. Adams, 2008: Rapid sampling of severe storms by the National Weather Radar Testbed Phased Array Radar. *Wea. Forecasting*, **23**, 808–824.

Jones, T. A., K. M. McGrath, and J. T. Snow, 2004: Association between NSSL mesocyclone detection algorithm-detected vortices and tornadoes. *Wea. Forecasting*, **19**, 872–890.

Lakshmanan, V., K. Hondl, and R. Rabin, 2009: An efficient, general-purpose technique for identifying storm cells in geospatial images. *J. Atmos. Oceanic Technol.*, **26**, 523–537.

Lakshmanan, V., R. Rabin, and V. DeBrunner, 2003: Multiscale storm identification and forecast. *Atmospheric Research*, **67-68**, 367–380.

Lakshmanan, V. and T. Smith, 2010: An objective method of evaluating and devising storm-tracking algorithms. *Wea. Forecasting*, **25**, 701–709.

Liu, S., M. Xue, and Q. Xu, 2007: Using wavelet analysis to detect tornadoes from Doppler radar radial-velocity observations. *J. Atmos. Oceanic Technol.*, **24**, 344–359.

Mitchell, E. D. W., S. V. Vasiloff, G. J. Stumpf, A. Witt, M. D. Eilts, J. T. Johnson, and K. W. Thomas, 1998: The National Severe Storms Laboratory tornado detection algorithm. *Wea. Forecasting*, **13**, 352–366.

Polger, P. D., B. S. Goldsmith, R. C. Przywarty, and J. R. Bocchieri, 1994: National Weather Service warning performance based on the WSR-88D. *Bull. Amer. Meteor. Soc.*, **75**, 203–214.

Rankine, W. J. M., 1901: *A Manual of Applied Mechanics*. 16th ed., Charles Griff and Co.

Smith, T. M. and K. L. Elmore, 2004: The use of radial velocity derivatives to diagnose rotation and divergence. Preprints, *11th Conf. on Aviation, Range and Aerospace*, Hyannis, MA. Amer. Meteor. Soc., P5.6.

Smith, T. M., K. L. Elmore, and S. A. Dulin, 2004: A damaging downburst prediction and detection algorithm for the WSR-88D. *Wea. Forecasting*, **19**, 240–250.

Stout, G. E. and F. A. Huff, 1953: Radar records Illinois tornadogenesis. *Bull. Amer. Meteor. Soc.*, **34**, 281–284.

Stumpf, G. J., A. Witt, E. D. Mitchell, P. L. Spencer, J. T. Johnson, M. D. Eilts, K. W. Thomas, and D. W. Burgess, 1998: The National Severe Storms Laboratory mesocyclone detection algorithm for the WSR-88D. *Wea. Forecasting*, **13**, 304–326.

Trapp, R. J., S. A. Tessendorf, E. S. Godfrey, and H. E. Brooks, 2005: Tornadoes from squall lines and bow echoes. Part I: Climatological distribution. *Wea. Forecasting*, **20**, 23–34.

Wang, Y. and T. Yu, 2009: Advanced tornado detection algorithm using super-resolultion and polarimetric data. Preprints, *34th Conf. on Radar Meteorology*, Williamsburg, VA. Amer. Meteor. Soc., P5.14.

Wang, Y., T.-Y. Yu, M. Yeary, A. Shapiro, S. Nemati, M. Foster, D. L. Andra, and M. Jain, 2008: Tornado detection using a neurofuzzy system to integrate shear and spectral signatures. *J. Atmos. Oceanic Technol.*, **25**, 1136–1148.

Wilks, D. S., 2006: *Statistical Methods in the Atmospheric Sciences*. 2d ed., Elsevier, New York, NY.

Wood, V. T. and R. A. Brown, 1997: Effects of radar sampling on single-Doppler velocity signatures of mesocyclones and tornadoes. *Wea. Forecasting*, **12**, 928–938.

Yu, T.-Y., Y. Wang, A. Shapiro, M. B. Yeary, D. S. Zrnić, and R. J. Doviak, 2007: Characterization of tornado spectral signatures using higher-order spectra. *J. Atmos. Oceanic Technol.*, **24**, 1997–2013.

Zrnić, D. S., D. W. Burgess, and L. D. Hennington, 1985: Automatic detection of mesocyclonic shear with Doppler radar. *J. Atmos. Oceanic Technol.*, **2**, 425–438.

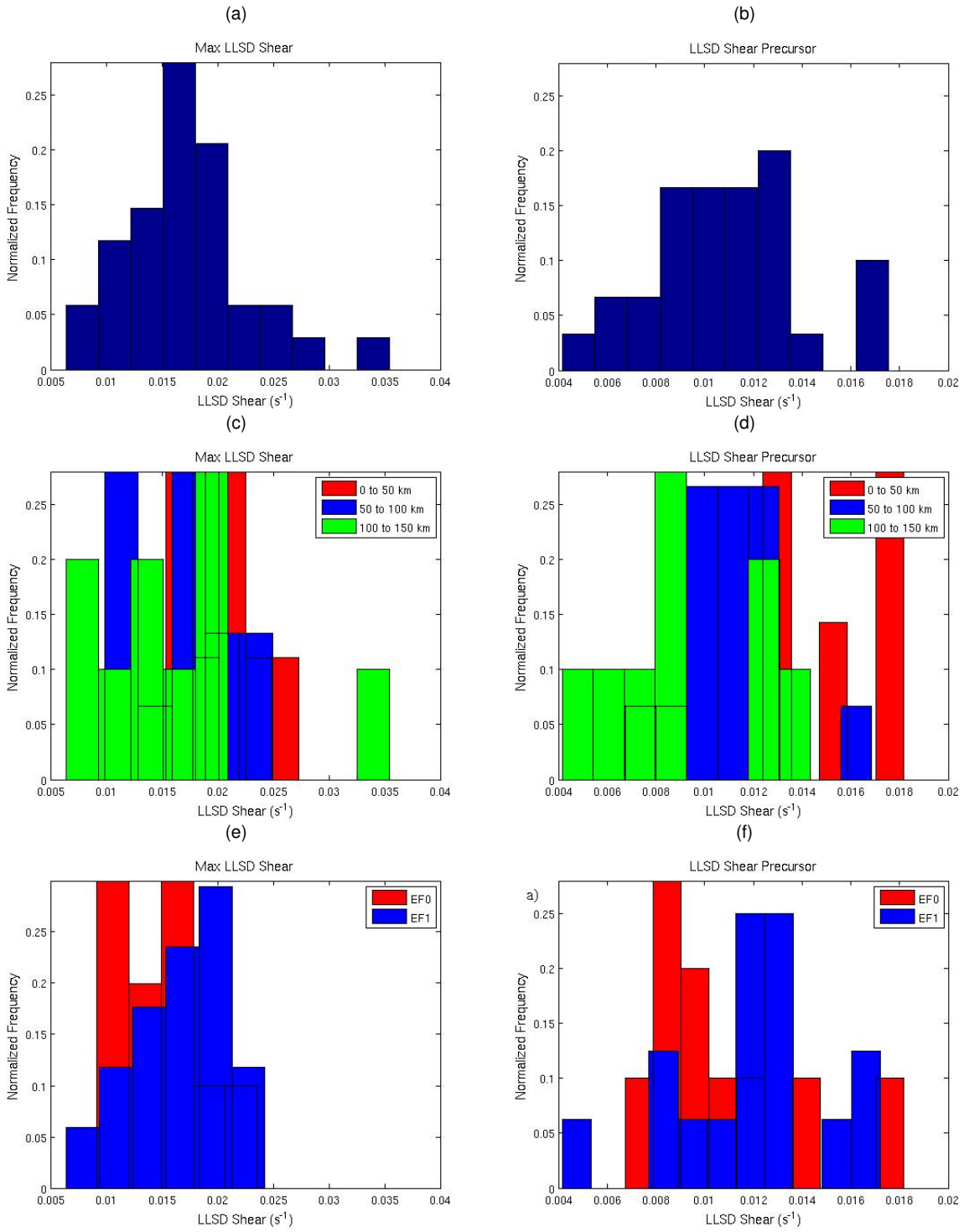

Figure 1: Normalized histograms of maximum and precursor LLSD shear values for tornado cases. c) and d) show histograms separated by tornado range. e) and f) show histograms separated by tornado intensity. Bin width for LLSD shear maximum histograms is 0.003 s^{-1}. Bin width for LLSD shear precursor histograms is 0.001 s^{-1}.

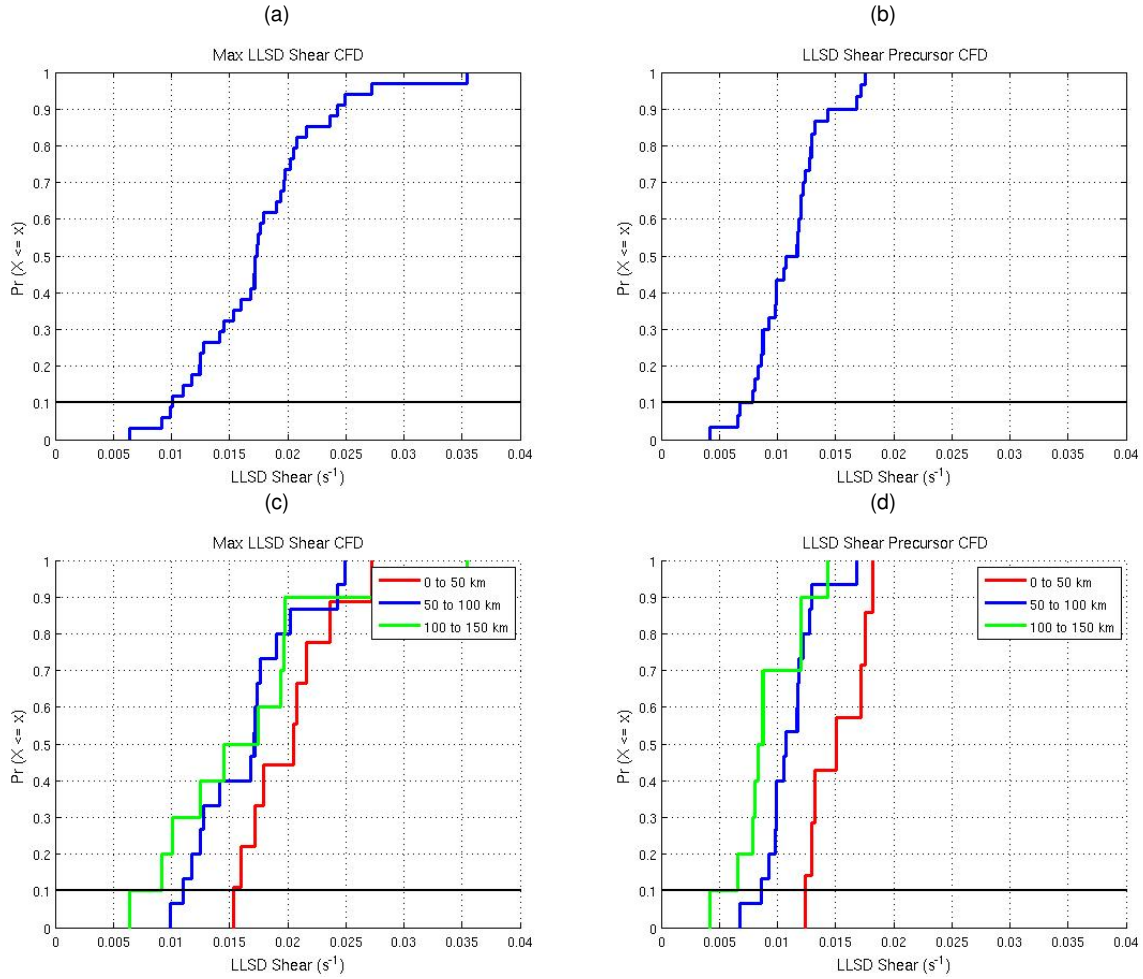

Figure 2: Cumulative frequency distribution functions for maximum and precursor LLSD shear values from tornado cases. c) and d) show functions separated by tornado range. The solid black line denotes the 0.1 (10%) probability that a future shear value will be lower than a given shear value.

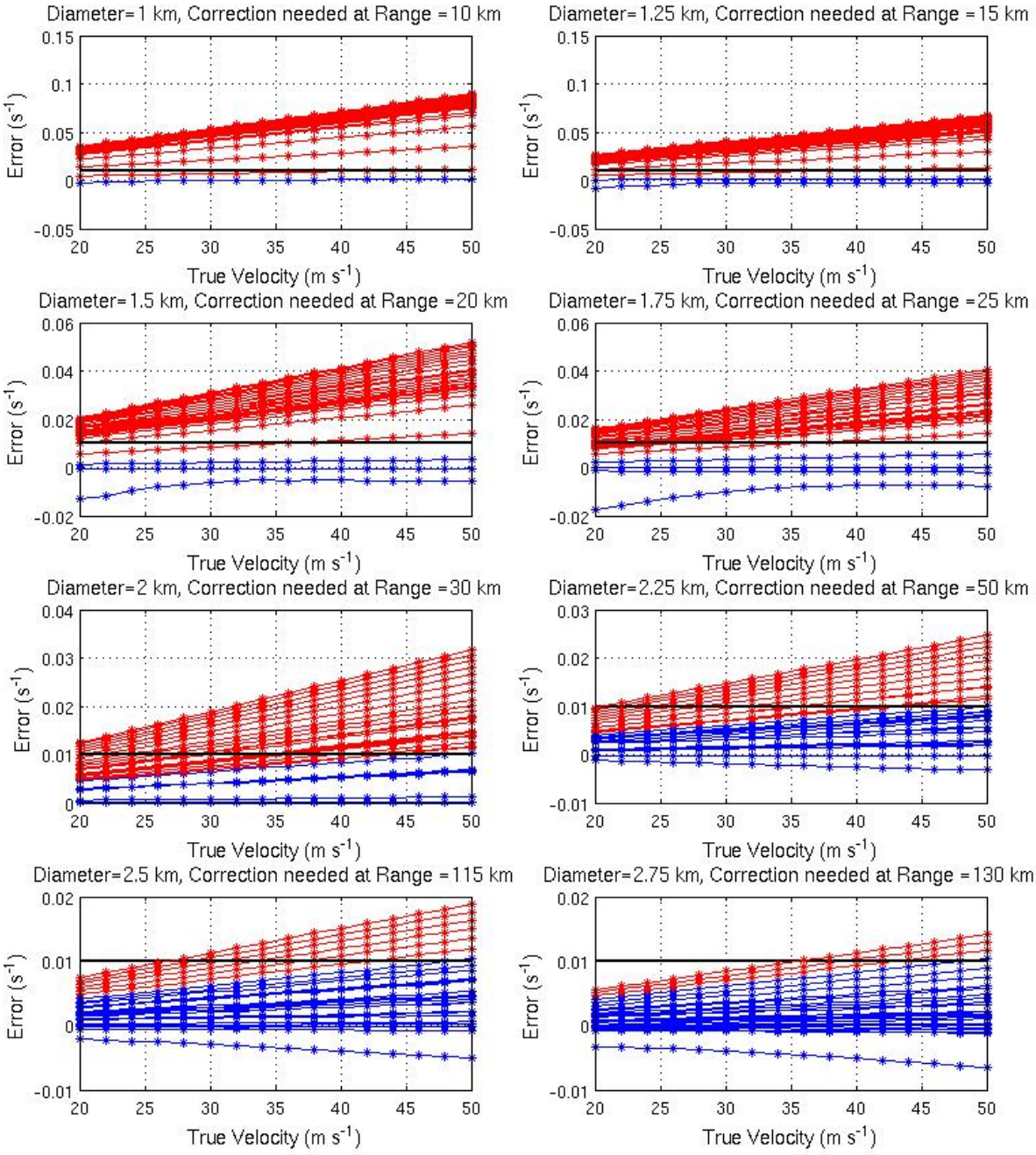

Figure 3: Shear error vs. true velocity for diameters from 1 to 2.75 km (circulations with diameters greater than 2.75 km did not require a range correction for ranges out to 140 km). Different lines in each plot correspond to errors at different ranges (5 to 140 km in increments of 5 km). Red lines indicate ranges for which the shear error exceeds 0.01 s^{-1} at three or more velocity points. These ranges define the location where a range correction is first needed for each diameter.

(a)

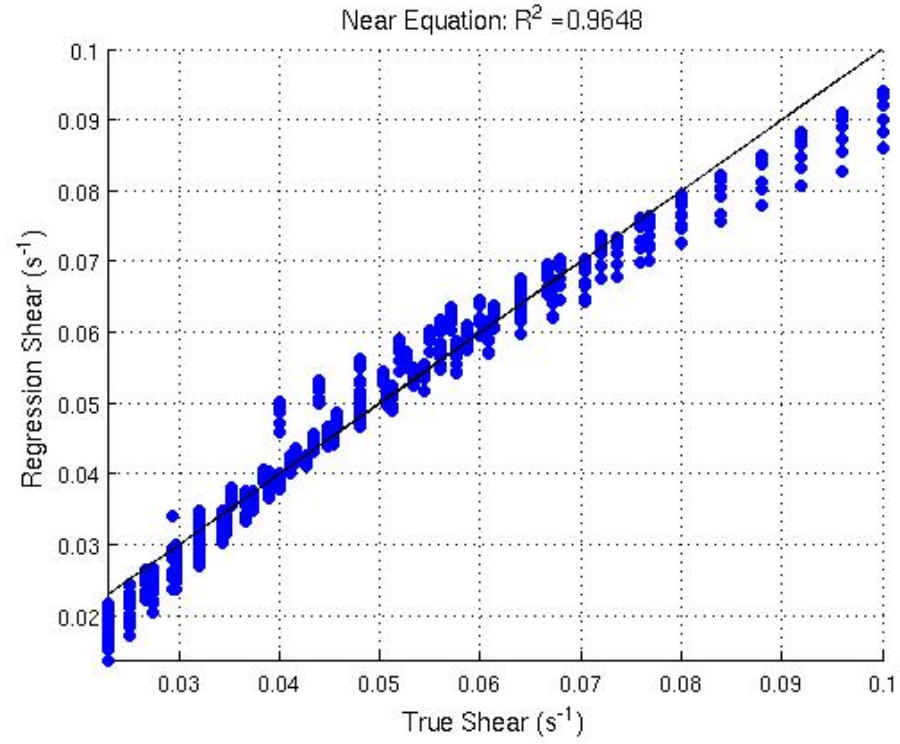

(b)

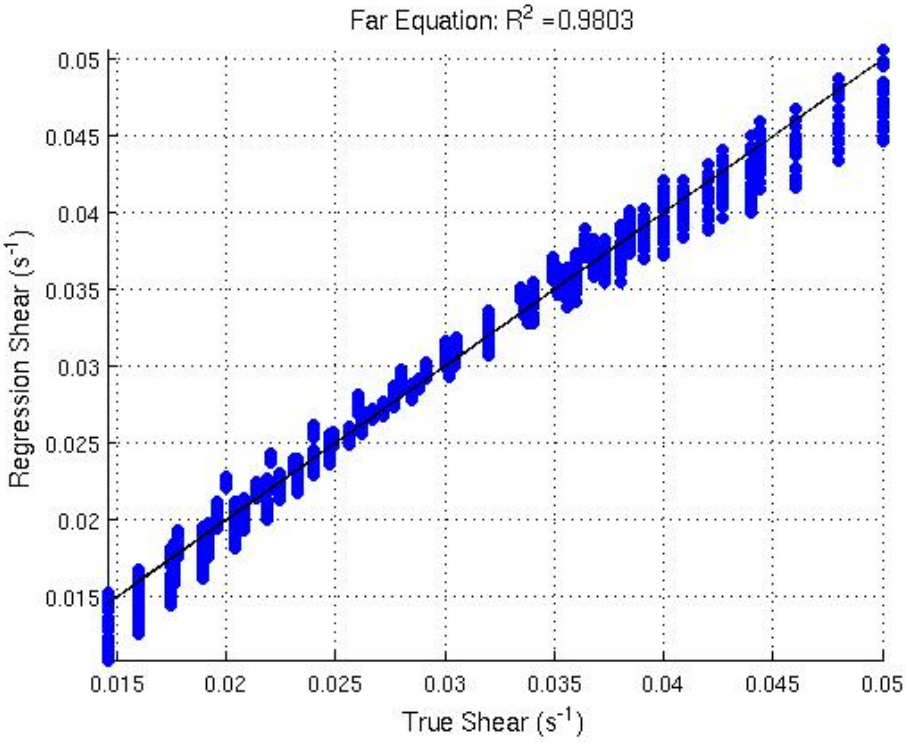

Figure 4: Results from near and far regression equations. Blue circles are corrected shear values calculated from the regression equation ("regression shear"). Black line shows location where corrected shear is equal to true shear (perfect fit).

(a)

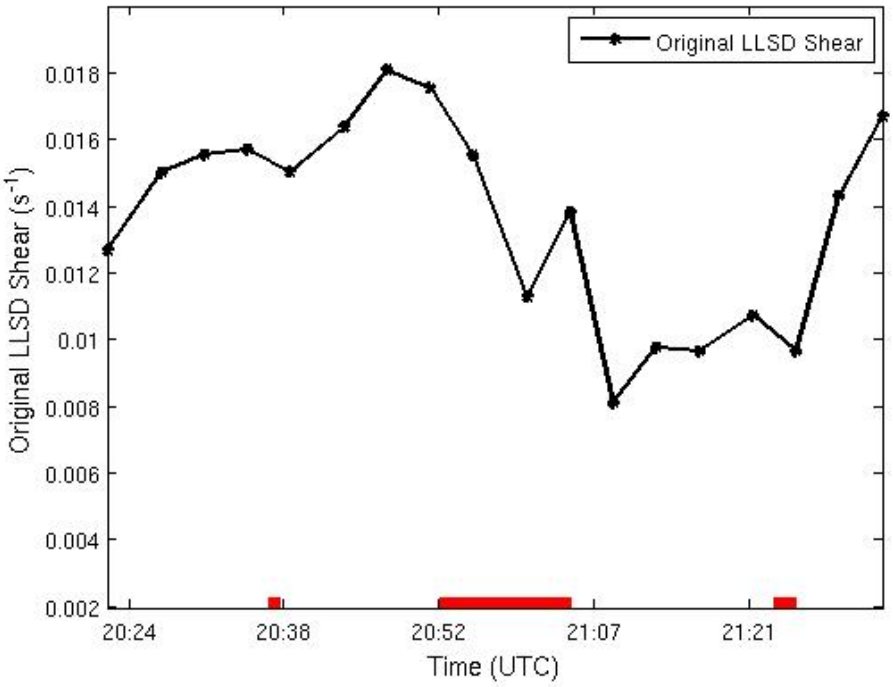

(b)

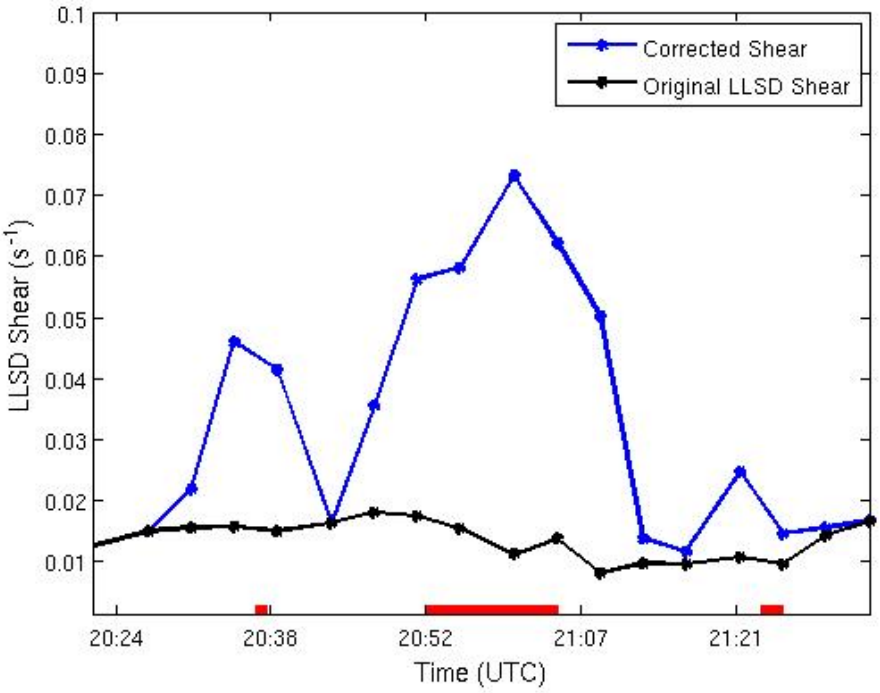

Figure 5: Original and corrected shear values for a cyclic supercell from the 10 February 2009 Oklahoma case. a) shows original uncorrected shear, and b) shows original and corrected shear on the same axis. Circles show actual times and shear values for low-level radar scans. Red lines denote approximate tornado times.

(a)

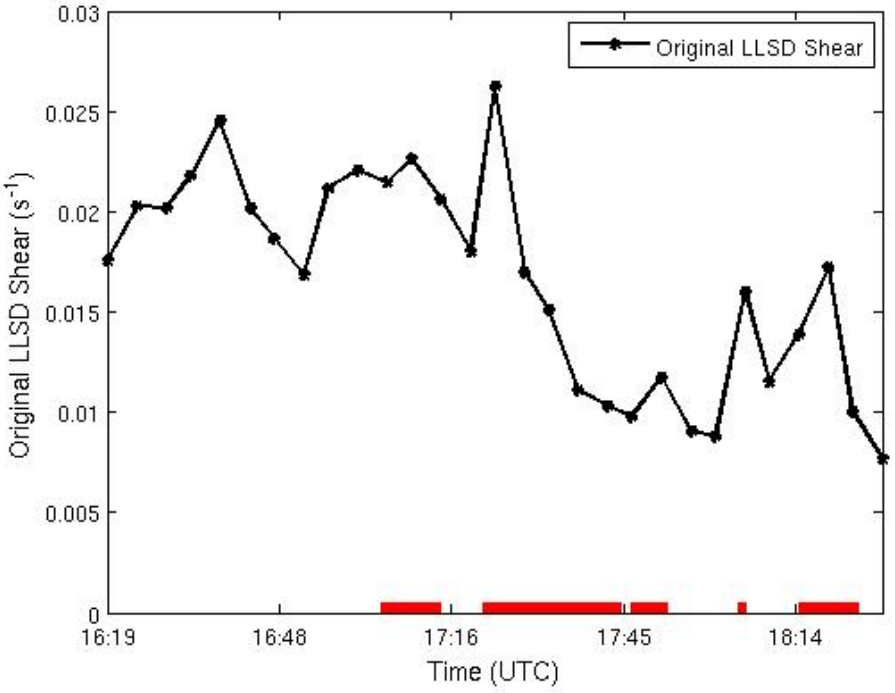

(b)

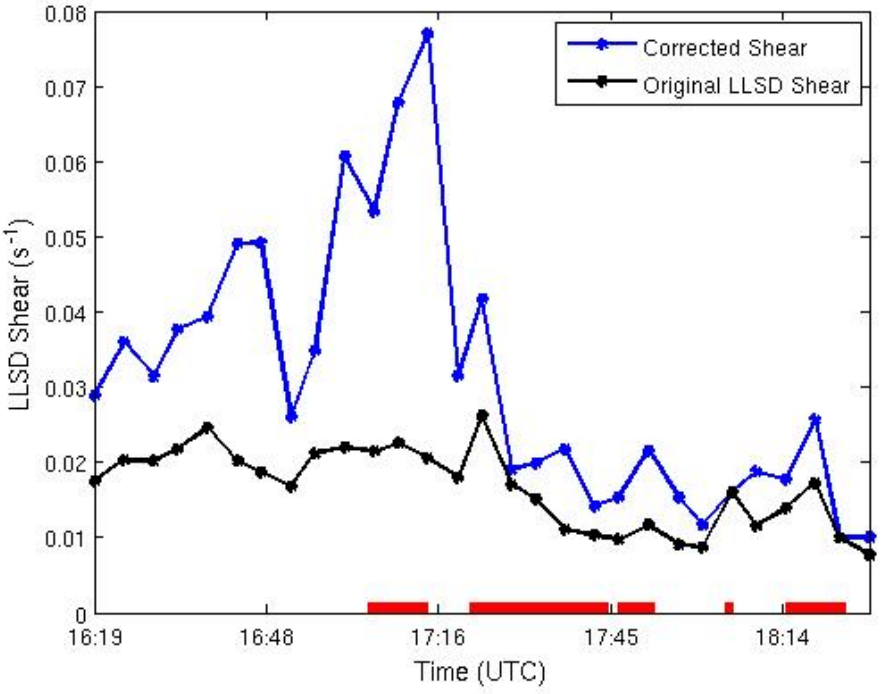

Figure 6: As in Fig. 5, but for 22 October 2009 Louisiana case.

Table 1: Tornado case dates and locations.

Date	State	Number of tornadoes
05/25/2008	Iowa	1
07/24/2008	New Hampshire	1
02/10/2009	Oklahoma	5
04/10/2009	Tennessee	7
04/19/2009	Alabama	7
08/19/2009	Illinois	4
08/19/2009	Iowa	1
10/22/2009	Louisiana	5

Table 2: Tornado intensities and ranges.

Intensity	Number of tornadoes
EF0	10
EF1	15
EF2	3
EF3	1
EF4	1
EF5	1
Range	**Number of tornadoes (% that were EF0 or EF1 tornadoes)**
0–50 km	7 (66.7)
50–100 km	14 (86.7)
100–150 km	10 (80)